Properties of evanescent waves in anisotropic media

Ilya Tsvankin

Center for Wave Phenomena, Department of Geophysics,

Colorado School of Mines, Golden, CO 80401-1887, USA.

E-mail: ilya@mines.edu.

(October 31, 2007)

ABSTRACT

Evanescent (inhomogeneous) waves contained in the plane-wave decomposition of point-source radiation produce not only surface waves but also nongeometrical modes that can be recorded far away from the boundary. This paper gives an analytic description of plane evanescent P-, SV-, and SH-waves propagating in the symmetry planes of non-attenuative transversely isotropic and orthorhombic media.

Simple weak-anisotropy approximations for the slowness and polarization vectors of horizontally traveling evanescent waves are obtained by linearizing the Christoffel equation in the anisotropy parameters. The relationship between the horizontal slowness (m_1) and the imaginary part of the vertical slowness (m_3) (i.e., between the horizontal velocity and the vertical amplitude decay factor) is controlled by the stiffness matrix. For P-waves, this relationship is sensitive even to relatively small values of the Thomsen parameters δ and, especially, ϵ. The weak-anisotropy approximation correctly reproduces the trend of the dependence of m_1 on m_3 for moderately anisotropic media, but deteriorates with increasing difference $\epsilon-\delta$, as the model deviates from elliptical. The influence of anisotropy on the function $m_1(m_3)$ is particularly significant for SV-waves because the slowness vector is governed by the parameter σ, which often exceeds 0.5. Anisotropy also distorts the particle motion of evanescent P- and SV-waves by changing the eccentricity of the polarization ellipse.

The results of this work can be used to develop asymptotic solutions for non-geometrical waves and design new anisotropic parameter-estimation algorithms for cross-hole and VSP surveys. In particular, measurements of the vertical decay factor of leaking waves traveling between boreholes can help to constrain the anisotropy parameters.

KEY WORDS: Evanescent waves, borehole data, slowness vector, particle motion, weak-anisotropy approximation, anisotropic media, transverse isotropy.

INTRODUCTION

A plane wave is called evanescent or inhomogeneous if at least one component of its slowness vector is complex. The imaginary part of the slowness vector causes spatial amplitude decay, with the planes of constant amplitude generally different from the planes of constant phase (i.e., from the wavefront). For example, plane waves are always evanescent in the presence of attenuation (absorption) because the stiffness tensor becomes complex. For non-attenuative media, evanescent waves are excited during reflection and transmission of conventional homogeneous plane waves when the angle of incidence exceeds the critical angle (e.g., Aki and Richards, 1980). Evanescent waves formed by transmission into thin high-velocity layers can become homogeneous upon leaving the layer and recorded far from the source, leading to so-called "tunneling" of energy (e.g., Červený and Aranha, 1992).

Also, plane-wave decomposition of point-source radiation always includes a range of evanescent plane waves whose velocities change continuously between zero and the medium velocity (Brekhovskikh, 1980). If the distance between the source and the nearest medium boundary is smaller than the predominant wavelength, evanescent energy contained in the point-source radiation gives rise to surface (Rayleigh, Stoneley) waves. Furthermore, evanescent plane waves can be transformed into homo-

geneous (non-decaying) waves during the reflection/transmission process, generating "nongeometrical" or "nonray" modes (Brekhovskikh, 1980; Tsvankin, 1995).

For example, if a point pressure source is located near a plane interface between two acoustic (fluid) media with the velocities c and c_1, the wavefield transmitted into the low-velocity halfspace contains two nongeometrical waves shown in Fig. 1. The wave P* is called "pseudospherical" because it has a spherical wavefront centered at the projection of the source onto the boundary (Brekhovskikh, 1980). According to Snell's law, the P*-wave can exist only in the post-critical domain between the boundary and the critical angle $\theta_{\rm cr} = \sin^{-1}(c_1/c)$. The second nongeometrical wave, $\bar{\rm P}$, is a "leaking" mode similar to conventional head waves (Phinney, 1961). It propagates along the boundary with a horizontal velocity slightly smaller than c and has a conical wavefront in the low-velocity halfspace. The take-off (transmission) angle i for the $\bar{\rm P}$-wave (Fig. 1) is close to the critical angle $\theta_{\rm cr}$.

Nongeometrical waves often produce intensive secondary reflected and head waves in layered media and, unlike surface waves, can be recorded far away from the boundary (Tsvankin, 1995). Because of nongeometrical phenomena, P-wave sources excite several intensive shear modes, such as the pseudospherical wave S* (Hron and Mikhailenko, 1981) and leaking waves propagating with shear-wave velocities (Tsvankin, 1995). This shear-wave energy can be of particular importance to anisotropic parameter-estimation algorithms that require a combination of P- and S-wave data (Tsvankin, 2005). Whereas it is well known that anisotropy has a strong influence on surface waves (Crampin and Taylor, 1971; Crampin, 1975), existing results for nongeometrical waves are restricted to isotropic models. To give an analytic description of nongeometrical phenomena in anisotropic media, it is necessary to study the properties of incident evanescent plane waves.

The goal of this paper is to build a foundation for analysis of nongeometrical modes in anisotropic media by obtaining closed-form expressions for the slowness and polarization vectors of evanescent waves. For simplicity, I consider plane waves

with the slowness vector confined to a symmetry plane of transversely isotropic (TI) or orthorhombic media. Linearization of the relationship between the horizontal and vertical slownesses (i.e., between the velocity and amplitude decay factor) helps to identify the combinations of the anisotropy parameters responsible for the properties of evanescent waves. Numerical tests for typical TI models confirm the strong influence of anisotropy on evanescent waves and help to evaluate the accuracy of the linearized solution.

CHRISTOFFEL EQUATION FOR EVANESCENT WAVES

Let us consider a harmonic plane wave propagating in a homogeneous, arbitrarily anisotropic medium:

$$u_n = U_n \, e^{i\omega(m_j x_j - t)} \,, \tag{1}$$

where $\mathbf{u}$ is the displacement vector, $\mathbf{U}$ is the unit polarization vector, ω is the angular frequency, and $\mathbf{m}$ is the slowness vector. If at least one of the components of the slowness vector is complex so that

$$m_j = m_j^{\mathrm{re}} + i m_j^{\mathrm{im}} \,, \tag{2}$$

the wave is called evanescent or inhomogeneous:

$$u_n = U_n \, e^{i\omega(m_j^{\mathrm{re}} x_j - t) - \omega m_j^{\mathrm{im}} x_j} \,. \tag{3}$$

To obtain the velocity, polarization, and amplitude decay factor of evanescent waves, the plane wave from eq. (3) should be substituted into the wave equation,

$$\rho \, \frac{\partial^2 u_i}{\partial t^2} - c_{ijkl} \, \frac{\partial^2 u_k}{\partial x_j \, \partial x_l} = 0 \,. \tag{4}$$

Here, ρ is the density and c_{ijkl} is the stiffness tensor, which is assumed to be real (i.e., the medium is non-attenuative); summation over repeated indices is implied. This

substitution results in the Christoffel equation, which has the same form as that for conventional homogeneous waves (e.g., Helbig, 1994; Tsvankin, 2005):

$$[c_{ijkl}\, m_j\, m_l - \rho\, \delta_{ik}]\, U_k = 0\,, \tag{5}$$

where $c_{ijkl}\, m_j\, m_l$ is usually called the Christoffel matrix and denoted by G_{ik}; δ_{ik} is Kronecker's symbolic δ. For evanescent waves, both the slowness and displacement vectors are generally complex. This means that the left-hand side of eq. (5) can be separated into the real and imaginary parts, which leads to coupled Christoffel equations for the vectors $\mathbf{m}$ and $\mathbf{U}$.

Carcione (2001) and Zhu and Tsvankin (2006) analyzed the Christoffel equation for attenuative anisotropic media (i.e., for complex c_{ijkl}), where the imaginary part $\mathbf{m}^{\rm im}$ of the slowness vector is often assumed to be parallel to the real part $\mathbf{m}^{\rm re}$ (wave propagation is then called "homogeneous"). The purpose of this work, however, is to study evanescent waves for purely elastic (non-attenuative) models. When the medium is elastic and isotropic, the real and imaginary parts of the slowness vector are perpendicular to each other. Indeed, for a purely isotropic tensor c_{ijkl}, eq. (5) reduces to the following coupled equations (Tsvankin, 1995):

$$|\mathbf{m}^{\rm re}|^2 = \frac{1}{V^2} + |\mathbf{m}^{\rm im}|^2\,, \tag{6}$$

$$\mathbf{m}^{\rm re} \cdot \mathbf{m}^{\rm im} = 0\,, \tag{7}$$

where V is the velocity of P- or S-waves. According to eq. (7), the direction of amplitude decay determined by $\mathbf{m}^{\rm im}$ is perpendicular to the wave-propagation direction $\mathbf{m}^{\rm re}$. The magnitude of $\mathbf{m}^{\rm im}$ has the meaning of the frequency-normalized amplitude decay factor of evanescent waves. The evanescent-wave velocity, which is equal to $1/|\mathbf{m}^{\rm re}|$, decreases from the medium velocity V to zero with increasing $|\mathbf{m}^{\rm im}|$ [eq. (6)].

Below I treat evanescent waves that propagate in the horizontal plane $[x_1, x_2]$ and decay in the vertical direction x_3. Plane evanescent waves of this type are contained

in Weyl-type integrals (i.e., in plane-wave decompositions of point-source radiation) used to solve reflection/transmission problems for horizontal interfaces (Brekhovskikh, 1980; Tsvankin and Chesnokov, 1990; Tsvankin, 1995, 2005). The medium is assumed to be transversely isotropic with a vertical symmetry axis (VTI), but the results are also valid in the symmetry planes of HTI (TI with a horizontal symmetry axis) and orthorhombic media where the Christoffel equation has the same form as for vertical transverse isotropy (Tsvankin, 2005).

Since VTI models are azimuthally isotropic and all vertical planes are equivalent, it is sufficient to consider the slowness vector confined to the coordinate plane $[x_1, x_3]$ (i.e., $m_2 = 0$):

$$\mathbf{m}^{\rm re} = \{m_1^{\rm re}, 0, 0\}\,, \quad \mathbf{m}^{\rm im} = \{0, 0, m_3^{\rm im}\}\,. \tag{8}$$

Then the plane wave from eq. (3) takes the form

$$u_n = U_n\, e^{i\omega(m_1 x_1 - t) - \omega m_3 x_3}\,. \tag{9}$$

Substituting the stiffness tensor for VTI media (e.g., Helbig, 1994) and the slowness vector from eq. (8) into the Christoffel equation (5) yields

$$[c_{11}(m_1^{\rm re})^2 - c_{55}(m_3^{\rm im})^2 - \rho\,]\,U_1 + i(c_{13}+c_{55})\,m_1^{\rm re}\,m_3^{\rm im}\,U_3 = 0\,, \tag{10}$$

$$[c_{66}(m_1^{\rm re})^2 - c_{55}(m_3^{\rm im})^2 - \rho\,]\,U_2 = 0\,, \tag{11}$$

$$i(c_{13}+c_{55})\,m_1^{\rm re}\,m_3^{\rm im}\,U_1 + [c_{55}(m_1^{\rm re})^2 - c_{33}(m_3^{\rm im})^2 - \rho\,]\,U_3 = 0\,. \tag{12}$$

For brevity, henceforth the superscripts "re" and "im" are omitted because the horizontal component of $\mathbf{m}$ is real, while the vertical component is imaginary.

EXACT SOLUTION FOR SH-WAVES

Since the slowness vector lies in a symmetry plane, SH-waves described by eq. (11) are decoupled from in-plane polarized P- and SV-waves [eqs. (10) and (12)]. The

SH-wave polarization vector is orthogonal to the propagation plane $[x_1, x_3]$, and the horizontal and vertical slownesses are related by [eq. (11)]

$$c_{66}\, m_1^2 - c_{55}\, m_3^2 - \rho = 0\,. \tag{13}$$

The horizontal slowness in eq. (13) can be expressed as

$$m_1^2 = \frac{1}{V_{\mathrm{hor,SH}}^2} + \frac{c_{55}}{c_{66}}\, m_3^2 = \frac{1}{1+2\gamma}\left(\frac{1}{V_{S0}^2} + m_3^2\right), \tag{14}$$

where $\gamma \equiv (c_{66} - c_{55})/(2c_{55})$ is the Thomsen (1986) anisotropy parameter responsible for SH-wave anisotropy, $V_{S0} = \sqrt{c_{55}/\rho}$ is the shear-wave vertical velocity, and $V_{\mathrm{hor,SH}}$ is the horizontal velocity of homogeneous SH-waves:

$$V_{\mathrm{hor,SH}} = \sqrt{\frac{c_{66}}{\rho}} = V_{S0}\sqrt{1+2\gamma}\,. \tag{15}$$

Setting $\gamma = 0$ makes eq. (14) identical to the corresponding isotropic expression 6. As in isotropic media, the velocity of evanescent SH-waves $(1/m_1)$ is smaller than the horizontal velocity $V_{\mathrm{hor,SH}}$ and decreases with increasing values of $|m_3|$. The contribution of γ, however, may substantially distort the realtionship between m_1 and m_3. Since typically $\gamma > 0$ (Wang, 2002), it increases the value of m_3^2 (and, therefore, of the amplitude decay factor) for a fixed horizontal slowness m_1.

SOLUTIONS FOR P- AND SV-WAVES

In the following, the discussion is focused on evanescent P- and SV-waves. Eqs. (10) and (12) cannot be solved simultaneously with a real displacement (polarization) vector **U**. Physically, this means that there is a phase shift between the vertical and horizontal polarization (displacement) components, and the polarization of evanescent waves is nonlinear. By analogy with known solutions for isotropic media (Tsvankin, 1995), this phase shift is expected to be equal to 90°, which corresponds to elliptical polarization. As shown below, introducing a 90° phase shift between the

polarization components is indeed sufficient to solve for the slownesses and polarizations of both P- and SV-waves. For simplicity, here the horizontal component U_1 is taken to be real and the vertical component U_3 imaginary. However, since eqs. (10) and (12) constrain only the *ratio* of the polarization components, both U_1 and U_3 can be complex, as long as their phase factors differ by 90°.

If U_1 is real and $U_3 = i|U_3|$, eqs. (10) and (12) become

$$(c_{11}m_1^2 - c_{55}m_3^2 - \rho)\, U_1 - (c_{13} + c_{55})\, m_1 m_3\, |U_3| = 0\,, \tag{16}$$

$$(c_{13} + c_{55})\, m_1 m_3\, U_1 + (c_{55}m_1^2 - c_{33}m_3^2 - \rho)\, |U_3| = 0\,. \tag{17}$$

To obtain a non-trivial solution, the determinant of the 2×2 matrix formed by the coefficients multiplied with U_1 and U_3 has to be set to zero:

$$(c_{11}m_1^2 - c_{55}m_3^2 - \rho)\,(c_{55}m_1^2 - c_{33}m_3^2 - \rho) + (c_{13} + c_{55})^2\, m_1^2\, m_3^2 = 0\,. \tag{18}$$

Note that eq. (18) becomes identical to the conventional equation for the slownesses of homogeneous P- and SV-waves in VTI media (e.g., Helbig, 1994) if m_3^2 is replaced by $-m_3^2$. As is the case for homogeneous waves, the slowness components m_1 and m_3 can be related to each other by solving a quadratic equation which follows from eq. (18). Such solutions play an important role in deriving reflection/transmission coefficients (e.g., Rüger, 2001) because all waves scattered at a horizontal interface have the same horizontal slowness according to Snell's law.

Weak-anisotropy approximation for P-waves

Relationship between the slownesses.—The exact expression for $m_1(m_3)$ (or vice versa) is not simple enough to reveal the contributions of the anisotropy parameters. As shown in Appendix A, a concise approximation can be obtained by applying perturbation approach and linearizing eq. (18) in the Thomsen (1986) parameters ϵ and δ. Henceforth, m_3 will be treated as a positive quantity, although (depending on

the sign of x_3) it can become negative to ensure exponential amplitude decay of the evanescent wave in eq. (9).

For the P-wave (i.e., for the solution with the smaller value of $|m_1|$ for a given $|m_3|$), the approximate horizontal slowness is given by

$$m_1^2 = \frac{1}{V_{\rm hor}^2} + m_3^2\,(1 - 4\epsilon + 2\delta) - 2m_3^4\,V_{P0}^2\,(\epsilon - \delta)\,, \tag{19}$$

where V_{P0} and $V_{\rm hor} = V_{P0}\,\sqrt{1+2\epsilon}$ are the vertical and horizontal velocities (respectively) of homogeneous P-waves. To make $m_1(m_3 = 0)$ exact, the term $1/V_{\rm hor}^2$ is not linearized in the parameter ϵ. In the absence of anisotropy ($\epsilon = \delta = 0$), eqs. (18) and (19) become equivalent to the isotropic expression (6):

$$m_1^2 = \frac{1}{V_{P0}^2} + m_3^2\,. \tag{20}$$

According to eq. (20), m_1 monotonically increases with m_3, so as the amplitude of evanescent waves decays faster in the vertical direction, their horizontal velocity decreases from V_{P0} to zero. It follows from eq. (19) that this general trend is preserved in the presence of moderate anisotropy (also, see the numerical examples below).

Still, even relatively small values of the parameters ϵ and δ may significantly change the velocity $V_{\rm hor}$ and the m_3^2-term in eq. (19), while the m_3^4-term is purely anisotropic. The multiplier of ϵ in the m_3^2-term is twice as large as that of δ because ϵ governs the P-wave velocity for near-horizontal directions. To separate the contribution of anisotropy to the linearized function $m_1(m_3)$, eq. (19) can be rewritten as

$$\frac{m_1^2}{1/V_{P0}^2 + m_3^2} = 1 - 2\epsilon - 2m_3^2\,V_{P0}^2\,(\epsilon - \delta)\,. \tag{21}$$

For evanescent waves with small values of the product $m_3 V_{P0}$ (i.e., with slow amplitude decay), the anisotropic term in eq. (21) is controlled primarily by ϵ. Since for typical TI models $\epsilon > 0$ and $\epsilon > \delta$ (Wang, 2002; Tsvankin, 2005), the influence of anisotropy reduces m_1 for a fixed value of m_3. This also means that for a given

horizontal slowness m_1, anisotropy increases m_3 and, therefore, the amplitude decay factor.

The above results indicate that the relationship between m_1 and m_3 can help in constraining the anisotropy parameters ϵ and δ; this issue is addressed in more detail below.

Numerical examples.—To evaluate the accuracy of the approximate relationship between m_1 and m_3, it is compared here with the exact solution for a representative set of VTI models. Numerical tests in Figs. 2 and 3 show that the error of eq. (19) strongly depends on the magnitude of the difference $\epsilon - \delta$, which quantifies the deviation from elliptical anisotropy. Note that P-wave time processing in VTI media is controlled by the anellipticity parameter $\eta = (\epsilon - \delta)/(1 + 2\delta) \approx \epsilon - \delta$ (Alkhalifah and Tsvankin, 1995). The weak-anisotropy approximation adequately predicts the general behavior of the exact solution even for strongly anisotropic elliptical models with equal values of ϵ and δ (Fig. 3). However, when $\epsilon > \delta$, the m_3^4-term in eq. (19) rapidly increases with m_3 and may yield unphysical values of m_1, which are smaller than $1/V_{\rm hor}$ (see the model with $\epsilon = 0.4$ and $\delta = 0.1$ in Fig. 3).

As expected, for a constant $\epsilon - \delta$, the error of the weak-anisotropy approximation increases with the absolute values of both anisotropy parameters. However, for typical weakly and moderately anisotropic models in Fig. 2b, eq. (19) is sufficiently close to the exact solution when m_3 is relatively small and correctly reproduces the trend of the function $m_1(m_3)$.

The above comparison of the exact and approximate solutions indicates that the linearized equation somewhat overstates the anisotropic contribution to the dependence of m_1 on m_3. Still, for typical models with $\epsilon > 0$ and $\epsilon - \delta \geq 0$, the anisotropic terms substantially reduce the slowness m_1 for a fixed value of m_3, as predicted by the weak-anisotropy approximation (19) (Fig. 4). In agreement with the exact expression (14) for elliptical anisotropy, the ratio of the VTI and isotropic values of m_1

is independent of m_3 when $\epsilon = \delta$ (Fig. 4a). For models with $\epsilon - \delta > 0$ (Fig. 4b), the difference between the VTI and isotropic results becomes more pronounced for larger values of m_3, which correspond to slower evanescent waves with a higher rate of amplitude decay.

Polarization ellipse.—Substitution of m_1 from eq. (19) into eqs. (16) or (17) yields the ratio of the polarization components U_1 and U_3, which determines the eccentricity of the polarization ellipse. Linearizing the result in the anisotropy parameters and the V_{S0}/V_{P0} ratio yields

$$\frac{|U_3|}{|U_1|} = \frac{m_3\, V_{P0}}{\sqrt{1 + m_3^2\, V_{P0}^2}} \left[1 - (\epsilon - \delta)(1 + m_3^2\, V_{P0}^2)\right] . \tag{22}$$

For a homogeneous P-wave with $m_3 = 0$, the displacement vector is horizontal ($U_3 = 0$), so the wave is polarized in the direction of propagation. The polarization becomes nonlinear with increasing m_3, and the anisotropic term that involves $\epsilon - \delta$ can make a substantial contribution to the polarization ellipse. Since typically $\epsilon - \delta > 0$, the influence of anisotropy in eq. (22) reduces the ratio $|U_3|/|U_1|$ and makes the polarization more linear.

Weak-anisotropy approximation for SV-waves

Relationship between the slownesses.—In principle, the approximate horizontal slowness for SV-waves can be derived in the same way as the one for P-waves by perturbing the isotropic expression for $m_1(m_3)$. Such a derivation, however, is unnecessary because any linearized kinematic (i.e., based entirely on slowness or velocity) signature for SV-waves can be obtained directly from the corresponding P-wave expression by making the following substitutions (Tsvankin, 2005): V_{P0} has to be replaced with V_{S0}, δ with the SV-wave velocity parameter $\sigma \equiv (V_{P0}^2/V_{S0}^2)\,(\epsilon - \delta)$, and ϵ set to zero. Applying this recipe to eq. (19) leads to

$$m_1^2 = \frac{1}{V_{S0}^2} + m_3^2\,(1 + 2\sigma) + 2m_3^4\, V_{S0}^2\, \sigma$$

$$= \frac{1}{V_{S0}^2} + m_3^2\,(1+2\sigma) + 2m_3^4\,V_{P0}^2\,(\epsilon-\delta)\,. \tag{23}$$

Anisotropy does not change the horizontal velocity of homogeneous SV-waves (it corresponds to $m_3 = 0$), which is equal to the vertical velocity V_{S0}. Since the parameter σ typically is positive (Wang, 2002; Tsvankin, 2005), its influence reduces m_3 and the amplitude decay factor for a fixed value of m_1. Because of the presence of the squared vertical-velocity ratio, the average value of σ for such common TI formations as shales exceeds 0.5 (Wang, 2002). Therefore, the contribution of anisotropy to the m_3^2-term is even more substantial for SV-waves than for P-waves. It is interesting that the factor $1+2\sigma$ in eq. (23) is also responsible for the SV-wave NMO velocity in VTI media (Thomsen, 1986; Tsvankin, 2005).

Polarization ellipse.—The linearized polarization ellipse for evanescent SV-waves has the form

$$\frac{|U_1|}{|U_3|} = \frac{m_3\,V_{S0}}{\sqrt{1+m_3^2\,V_{S0}^2}}\,\left[1-(2\epsilon-\delta)-2\sigma\,m_3^2\,V_{S0}^2\right]\,. \tag{24}$$

The polarization vector for a homogeneous SV-wave ($m_3 = 0$) is vertical; the horizontal displacement component increases with m_3. According to eq. 24, the anisotropic terms typically reduce the ellipticity of the SV-wave polarization, which was also the case for P-waves.

DISCUSSION AND CONCLUSIONS

Evanescent waves play an important role inm_1 and m_3 a number of wave-propagation problems, such as generation of nongeometrical modes by sources located close to medium interfaces. This paper introduces concise weak-anisotropy approximations for the slowness and polarization vectors of evanescent plane waves that propagate in the horizontal (isotropy) plane of VTI media. The results remain entirely valid for wave propagation along the intersections of the symmetry planes of orthorhombic and HTI media.

The velocity of evanescent waves can take any value smaller than the horizontal velocity of the corresponding (i.e., P, SV, or SH) homogeneous wave. By solving the Christoffel equation, one can relate the evanescent-wave velocity (or the horizontal slowness m_1) to the vertical slowness m_3, which governs the amplitude decay factor. While the exact relationship between m_1 and m_3 for SH-waves is rather simple and involves a single anisotropy parameter (γ), it is much less transparent for P- and SV-waves. To explain the contribution of anisotropy to both the slowness and polarization vectors of evanescent P- and SV-waves, the solutions of the Christoffel equation were linearized in the parameters ϵ and δ.

The anisotropic terms in the approximate P-wave function $m_1(m_3)$ include both ϵ and δ, although the sensitivity to ϵ is higher. Even for relatively small values of ϵ and δ on the order of 0.1–0.15, the influence of anisotropy on the relationship between m_1 and m_3 is significant, especially for evanescent waves with smaller velocities and higher amplitude decay rates. For typical VTI models with $\epsilon > 0$ and $\epsilon > \delta$, the decay factor governed by m_3 can be much larger than that in isotropic media for the same value of m_1. Numerical testing demonstrates that the accuracy of the weak-anisotropy approximation for the dependence $m_1(m_3)$ is mostly governed by the difference $\epsilon - \delta$, rather than by either parameter individually.

The linearized relationship $m_1(m_3)$ for SV-waves was obtained as a special case of the P-wave result by applying the "substitution rule" described in Tsvankin (2005) for homogeneous waves. In contrast to P-waves, the influence of anisotropy reduces the amplitude decay factor of SV-waves for a given m_1. The anisotropic terms in the function $m_1(m_3)$ are controlled by the SV-wave velocity parameter σ, which often reaches large values exceeding 0.5.

The polarization of evanescent P- and SV-waves becomes increasingly nonlinear (elliptical) with a reduction in their horizontal velocity. The weak-anisotropy approximation for the ratio of the vertical and horizontal displacements shows that for both P- and SV-waves the contribution of ϵ and δ typically decreases the eccentricity of

the polarization ellipse.

These results will help to develop asymptotic solutions for nongeometrical waves in anisotropic media using, for example, the stationary-phase method. In particular, the description of evanescent waves given above is directly applicable to leaking waves (Fig. 1) excited by buried (e.g., borehole) sources at internal boundaries.

As discussed in Tsvankin (1995), the dependence of the horizontal velocity on the amplitude decay factor of evanescent waves [i.e., the function $m_1(m_3)$] can be measured by recording leaking waves in cross-hole or reverse VSP (vertical seismic profiling) surveys. To estimate the decay factor of a leaking wave, the source should be moved along the borehole while keeping the receiver position fixed. The strong influence of the anisotropy parameters on the dependence $m_1(m_3)$ indicates that leaking modes can be effectively used to constrain anisotropic velocity fields. In particular, the relationship between m_1 and m_3 in cross-hole data can help to estimate the parameter δ, which is poorly resolved by conventional cross-hole tomography.

ACKNOWLEDGMENTS

I am grateful to my colleagues at the Center for Wave Phenomena (CWP), Colorado School of Mines (CSM), for useful discussions and to Jyoti Behura (CSM) for help with the numerical examples. Reviews by Roel Snieder and Yaping Zhu (both CSM) helped to improve the manuscript. The support for this work was provided by the Consortium Project on Seismic Inverse Methods for Complex Structures at CWP and by the Chemical Sciences, Geosciences and Biosciences Division, Office of Basic Energy Sciences, Office of Science, U.S. Department of Energy.

REFERENCES

Aki, K. and Richards, P. G., 1980. Quantitative Seismology. Theory and Methods. W. N. Freeman & Co.

Alkhalifah, T. and Tsvankin, I., 1995. Velocity analysis in transversely isotropic media. Geophysics, 60: 1550–1566.

Brekhovskikh, L. M., 1980. Waves in Layered Media. Academic Press.

Carcione, J. M., 2001. Wave Fields in Real Media: Wave propagation in Anisotropic, Anelastic, and Porous media. Pergamon Press.

Červený, V. and Aranha, P. R. A., 1992. Tunneling of seismic body waves through thin high-velocity layers in complex structures. Studia Geophys. and Geod., 36: 115–138.

Crampin, S., 1975. Distinctive particle motion of surface waves as a diagnostic of anisotropic layering. Geophys. J. R. Astr. Soc., 40: 177–186.

Crampin, S. and Taylor, D. B., 1971. The propagation of surface waves in anisotropic media. Geophys. J. R. Astr. Soc., 25: 71–87.

Helbig, K., 1994. Foundations of Elastic Anisotropy for Exploration Seismics. Pergamon Press.

Hron, F. and Mikhailenko, B. G., 1981. Numerical modeling of nongeometrical effects by the Alekseev-Mikhailenko method. Bull. Seismol. Soc. Amer., 71: 1011–1029.

Phinney, R. A., 1961. Propagation of leaking interface waves. Bull. Seismol. Soc. Amer., 51: 527–555.

Rüger, A., 2001. Reflection Coefficients and Azimuthal AVO Analysis in Anisotropic Media. Society of Exploration Geophysicists.

Thomsen, L., 1986. Weak elastic anisotropy. Geophysics, 51: 1954–1966.

Tsvankin, I., 1995. Seismic Wavefields in Layered Isotropic Media. Samizdat Press, Colorado School of Mines.

Tsvankin, I., 2005. Seismic Signatures and Analysis of Reflection Data in Anisotropic Media, 2nd Edition. Elsevier Science Publ. Co., Inc.

Tsvankin, I. and Chesnokov, E. M., 1990. Synthesis of body wave seismograms from point sources in anisotropic media. J. Geophys. Res., 95(B7): 11317–11331.

Wang, Z., 2002. Seismic anisotropy in sedimentary rocks, part 2: Laboratory data. Geophysics, 67: 1423–1440.

Zhu, Y. and Tsvankin, I., 2006. Plane-wave propagation in attenuative transversely isotropic media. Geophysics, 71: T17–T30.

APPENDIX A–LINEARIZED RELATIONSHIP BETWEEN THE SLOWNESSES OF EVANESCENT WAVES

The horizontal slowness m_1 of evanescent waves can be expressed as a function of the imaginary part m_3 of the vertical slowness (m_3 represents the frequency-normalized decay factor) by solving eq. (18). To develop the weak-anisotropy approximation for the function $m_1(m_3)$, it is convenient to replace the stiffness coefficients in eq. (18) by the parameters ϵ and δ:

$$c_{11} = V_{P0}^2 \rho \left(1 + 2\epsilon\right), \tag{A-1}$$

$$c_{33} = V_{P0}^2 \rho, \tag{A-2}$$

$$c_{55} = V_{S0}^2 \rho, \tag{A-3}$$

$$(c_{13} + c_{55})^2 = V_{P0}^4 \rho^2 f \left(2\delta + f\right), \tag{A-4}$$

where $f \equiv 1 - V_{S0}^2/V_{P0}^2$ is a useful parameter combination introduced by Tsvankin (2005).

The isotropic solutions for $m_1(m_3)$ are obtained by setting $\epsilon = \delta = 0$ and substituting eqs. (A-1)–(A-4) into eq. (18):

$$m_1^2 = \frac{1}{V^2} + m_3^2, \tag{A-5}$$

with the medium velocity V equal to V_{P0} for P-waves and V_{S0} for S-waves.

The weak-anisotropy approximation can be derived by perturbing the isotropic expression (A-5). For P-waves, such a perturbation can be written as

$$m_1^2 = \frac{1}{V_{P0}^2} + m_3^2 + \Delta(m_1^2), \tag{A-6}$$

where $\Delta(m_1^2)$ is a linear function of ϵ and δ. Substituting m_1^2 from eq. (A-6) into eq. (18) and keeping only the linear terms in the anisotropy parameters yields

$$\Delta(m_1^2) = -2\epsilon\,\frac{(1+m_3^2\,V_{P0}^2)^2}{V_{P0}^2} + 2\delta\,m_3^2\,(1+m_3^2\,V_{P0}^2)\,. \tag{A-7}$$

The linearized approximation for m_1^2 is then obtained from eq. (A-6) as

$$m_1^2 = \frac{1}{V_{\rm hor}^2} + m_3^2\,(1-4\epsilon+2\delta) - 2m_3^4\,V_{P0}^2\,(\epsilon-\delta)\,; \tag{A-8}$$

$V_{\rm hor} = V_{P0}\,\sqrt{1+2\epsilon}$ is the P-wave horizontal velocity. The term $1/V_{\rm hor}^2$ is not linearized in ϵ to keep the horizontal slowness exact for $m_3 = 0$.

FIGURES

FIG. 1. Asymptotic "raypaths" of the pseudospherical wave P* and leaking wave $\bar{\text{P}}$ generated at the boundary between two acoustic halfspaces with the velocities c and c_1 ($c > c_1$). The amplitudes of both nongeometrical waves decay exponentially between the source and the boundary. The traveltime of the $\bar{\text{P}}$-wave almost coincides with that of the conventional transmitted P-wave, while the wave P* forms a later arrival (after Tsvankin, 1995).

FIG. 2. Comparison of the exact function $m_1(m_3)$ from eq. 18 (solid curves) with the weak-anisotropy approximation 19 (dashed) for elliptical (a) and non-elliptical (b) VTI models. The error of the approximation becomes larger with increasing values of $\epsilon - \delta$. Both slowness components are multiplied with the velocity V_{P0} to make them dimensionless.

FIG. 3. Comparison of the exact (solid curves) and approximate (dashed) functions $m_1(m_3)$ for two models with strong velocity anisotropy.

FIG. 4. Influence of anisotropy on the relationship between the horizontal and vertical slownesses for the models from Fig. 2. The exact slowness m_1 computed from eq. 18 is normalized by the isotropic value that corresponds to $\epsilon = \delta = 0$. The shape of the normalized curves is qualitatively described by the weak-anisotropy approximation 21.

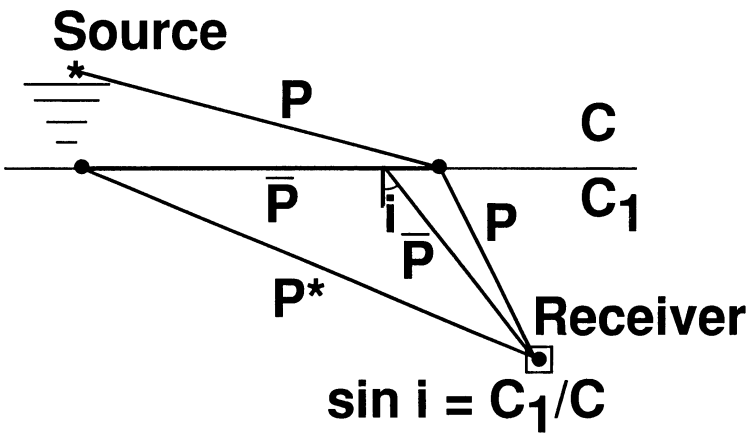

FIG. 1. Asymptotic "raypaths" of the pseudospherical wave P* and leaking wave $\bar{\text{P}}$ generated at the boundary between two acoustic halfspaces with the velocities c and c_1 ($c > c_1$). The amplitudes of both nongeometrical waves decay exponentially between the source and the boundary. The traveltime of the $\bar{\text{P}}$-wave almost coincides with that of the conventional transmitted P-wave, while the wave P* forms a later arrival (after Tsvankin, 1995).

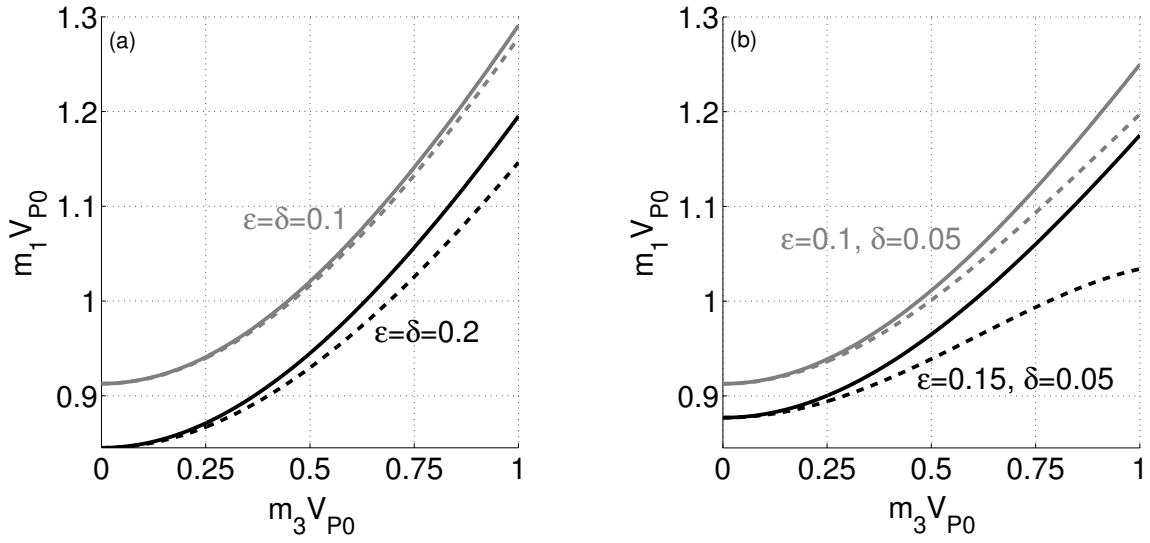

FIG. 2. Comparison of the exact function $m_1(m_3)$ from eq. 18 (solid curves) with the weak-anisotropy approximation 19 (dashed) for elliptical (a) and non-elliptical (b) VTI models. The error of the approximation becomes larger with increasing values of $\epsilon - \delta$. Both slowness components are multiplied with the velocity V_{P0} to make them dimensionless.

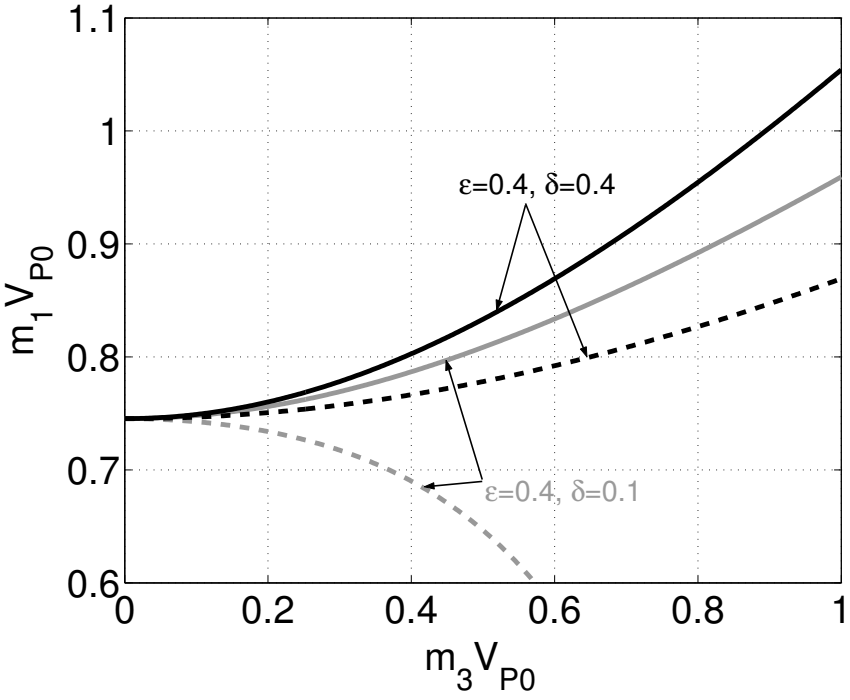

FIG. 3. Comparison of the exact (solid curves) and approximate (dashed) functions $m_1(m_3)$ for two models with strong velocity anisotropy.

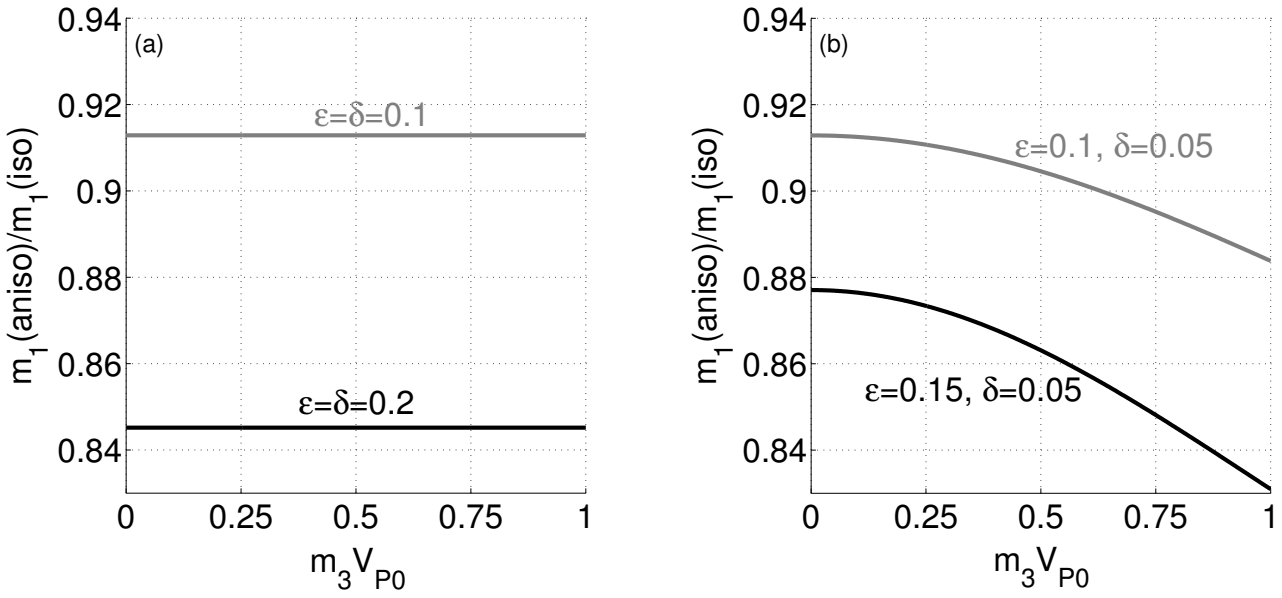

FIG. 4. Influence of anisotropy on the relationship between the horizontal and vertical slownesses for the models from Fig. 2. The exact slowness m_1 computed from eq. 18 is normalized by the isotropic value that corresponds to $\epsilon = \delta = 0$. The shape of the normalized curves is qualitatively described by the weak-anisotropy approximation 21.